Desalination and Water Treatment
www.deswater.com
doi: 10.5004/dwt.2019.23219

142 (2019) 1–10
February

Numerical simulation and experimental validation of a compact distillation module used in solar desalination unit

Khalifa Zhani[a,b]

[a]*Mechanical Department, College of Engineering, University of Bisha, Bisha, Saudi Arabia; email: kzhani@ub.edu.sa*
[b]*Laboratoire des Systemes Electro-Mecaniques (LASEM), National Engineering School of Sfax, B.P. W3038, Sfax, Tunisia*

Received 4 May 2018; Accepted 28 September 2018

ABSTRACT

Fresh water production of solar desalination system is most influenced by the distillation module performance. In this paper, we propose a new design of a compact distillation module used in a desalination unit. The desalination process is based on humidification–dehumidification principle. In order to be able to simulate the dynamic behavior of the distillation module exposed to a variation of entrance parameters, a mathematical model is developed in dynamic regime from the governing heat and mass transfer equations in both the evaporation chamber and the condensation chamber. The obtained distributed systems of equations are transformed into a system of ordinary differential equations using the orthogonal collocation method. The theoretical study shows the effects of operating parameters on the performance of the distillation module. The experimental validation shows a good agreement between predicted and measured parameters.

Keywords: Solar desalination; Humidification–dehumidification; Simulation; Experimental validation

1. Introduction

Water is one of the most abundant resources on earth, covering three fourths of the planet's surface. However, there is a shortage of fresh water in many regions worldwide. Regions facing the scarcity of fresh water resources are dry regions where solar energy is abundant. Considering the limitations and available resources of dry areas throughout the world, a standard solution widely in use is desalination using solar energy technology. Environmentally, the solar energy harnessing system has advantages as it vanishes pollution into the atmosphere as they are with the combustion of fossil fuels. Thus, as a long-term option, the solar energy system can be considered as an alternative to all the finite fuel system. Several countries throughout the world have experimented with the application of solar energy to desalination processes where they use solar still to produce freshwater.

Classical solar desalination systems, such as those using solar still, have often been reported to entail some limitations [1–7]. The most prohibitive drawback of a solar stills is their low efficiency (gained output ratio <0.5) which is primarily the result of the immediate loss of the latent heat of condensation through the glass cover of the still. Several experimental and theoretical studies have recently reported that other more promising solar desalination techniques that are based on the humidification–dehumidification principle have been developed for the production of freshwater in remote and sunny regions. Solar desalination units based on humidification–dehumidification principle are characterized by their limited production of fresh water. So, to optimize the functioning and then the productivity of solar desalination units, we should first study in depth the behavior of each component constituting the unit. For this purpose, according to the literature review, many investigators have developed and investigated theoretically and experimentally different elements of various solar desalination systems using the humidification and dehumidification principle.

* Corresponding author.

Behnam and Shafii [8] have developed a novel solar humidification technique incorporating the heating of water, the heating of the air stream and the humidification of air in one compact unit to improve the performance of solar humidification and dehumidification desalination systems while at the same time reducing the size of the whole system. The effects of various parameters including the incoming air flow rate into the humidifier and the first depth of water in the humidifier have been studied. It was found that increasing the inlet air flow rate to the humidifier and initial water depth in the later equal to the length of the heat pipe condenser inside the humidifier increase daily fresh water production. They reported that the daily fresh water productivity and the daily efficiency increased significantly and reached 6.275 kg/d m^2 and 65%. The cost of fresh water produced through the presented system is estimated to be 0.028 $/L.

Muthusamy and Srithar [9] developed an experimental investigation to enhance the fresh water production of the humidification–dehumidification desalination system. The studied desalination system includes an air heater, water heater, humidifier and condenser. They tested two types of packing materials such as gunny bag and saw dust in the humidifier region to improve the mass transfer mechanism. It was found that the gunny bag gives a higher mass transfer rate inside the humidifier. They inserted into the condenser spring for pitch ratios of 3 and 4 in order to enhance the overall heat transfer coefficient in the condenser. They revealed that, for the same input power, the improved system boosted the heat exit and productivity equivalent to a power saving of 40% and 13%, respectively.

Malek [10] studied the effect of condenser unit attached to the passive solar still on the daily productivity and carried out a comparative study for passive solar still and condenser connected to the solar still. It has been observed that condenser attachment gives the higher productivity as compared to the passive solar still. In the same year, Tow and Lienhard [11] have studied the heat flux experimentally and parallel flow effectiveness of a bubble column condenser using significantly smaller cooling coils. In addition, they have developed a mathematical model which predicts the heat transfer rate with an average error of less than 3%. It is found that heat flux rises and effectiveness decreases with decreasing coil area. Increasing both the air flow rate and air temperature lead to increased heat flux but reduced efficiency.

The distillation module is the most complicated component of the solar desalination unit since it involves the two reverse physical phenomena (humidification and dehumidification). Furthermore, the humidification/dehumidification process is actually a multiphase flow, with phase change and simultaneous mass and heat transfer between the phases. As shown in Fig.1, the heat transfer between water and air can be divided into two categories according to the direction of the mass transfer, heat transfer with humidification (evaporation) and heat transfer with dehumidification (condensation). They have the following differences [12]: (i) in humidification, the heat and mass move in opposite directions, while in dehumidification, they have the same direction; (ii) the vapor enters the interface at the water temperature in case of evaporation while it enters the interface at the air temperature in case of condensation; (iii) the air film is thicker in case of evaporation but thinner in case of condensation; (iiii) condensation commences when the partial pressure of water vapor in the air phase is higher than the partial pressure at the interface while evaporation starts when the partial pressure of water vapor at the interface is higher than the corresponding partial pressure in the air phase.

The developed solar desalination system using the humidification–dehumidification principle includes five components: water and air solar collectors, humidifier and the distillation module. In two previous papers [13,14], we have presented the detailed study of the air and water solar collectors and the humidifier. The current paper deals with the distillation module study. Its underlying objectives are as follows:

- To present the design of the distillation module.
- To develop and validate a dynamic mathematical model able to predict the thermal performance of the distillation module.
- To study the effects of operating and design parameters on the performance of the distillation module.

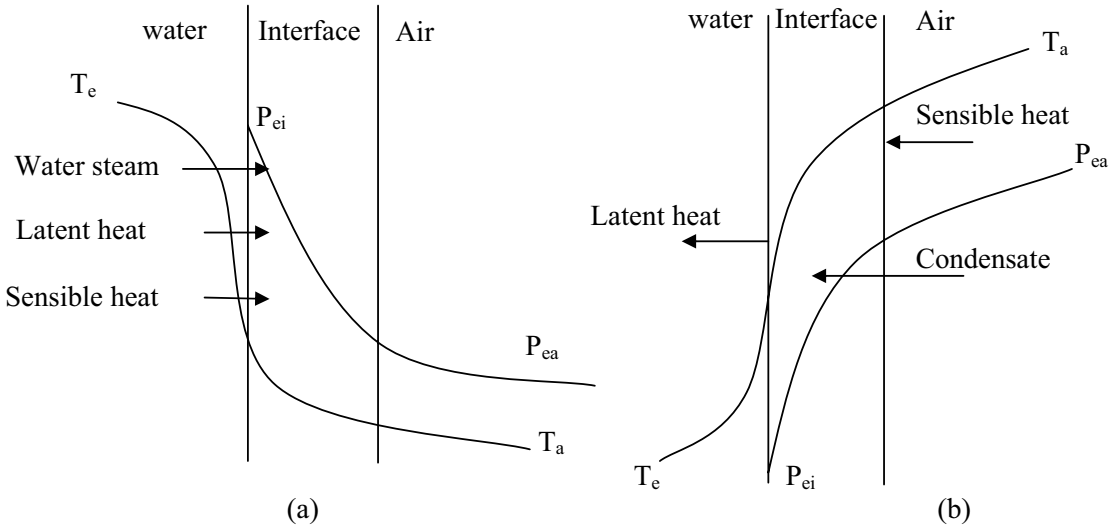

Fig. 1. Heat transfer with humidification (a) and with dehumidification (b).

2. Distillation module design

Fig. 2 presents the design of the distillation module. The latter consists of the air humidifier (evaporation chamber) and dehumidifier (condensation chamber). There is no wall separating the two chambers. In order to ensure the long-term operation of the distillation module, the evaporation chamber and the condensation chamber are well designed and realized. The condensation chamber is constituted of 12 dismantled vertical rows, to ensure its maintenance, and arranged in a triangular arrangement. Each row contains 12 circular tubes in copper of inner diameter 12 mm and outer diameter 14 mm, and its length is 1.5 m. The transverse and the longitudinal pitch are designated, respectively, by 50 and 50 mm. The evaporation chamber consists of 12 horizontal tubes made in copper of inner diameter 20 mm and outer diameter 22 mm equipped with small holes (1.5 mm diameter) provided on the higher surface of the tube. The holes work as pulverizers that pulverize the hot salt water. To augment the contact surface between air and water, thus, to increase the evaporation rate and to prevent pulverized hot salt water at the top of the evaporation chamber to be mixed with the fresh water at the bottom of condensation chamber, each horizontal tube mentioned previously is covered with a textile of exchange surface 49 m². Table 1 summarizes the properties of the distillation module used in the simulation.

The principle of functioning of the distillation module is as follows: hot salt water coming from the solar water collector enters the module at the top of the evaporation tower. The packed bed absorbs it (textile of viscose). Due to heat and mass transfers between the hot water and the partially dehumidified air stream exiting the condensation tower at the bottom, air is loaded with moisture. The saturated moist air is then drifted toward the tower of condensation by natural convection where it enters in contact with a surface, the temperature of which is lower than the dew point of the air. The natural convection occurs when a solid surface is in contact with a fluid of different temperatures from the surface. Density differences provide the body force required to move the fluid. The condensed water was collected from the bottom of the condensation tower, while the brine (the salty water exiting the evaporator) at the bottom of the evaporation tower will be either recycled and combined with the feed solution at the entry point or rejected in case of an increase of saltiness rates.

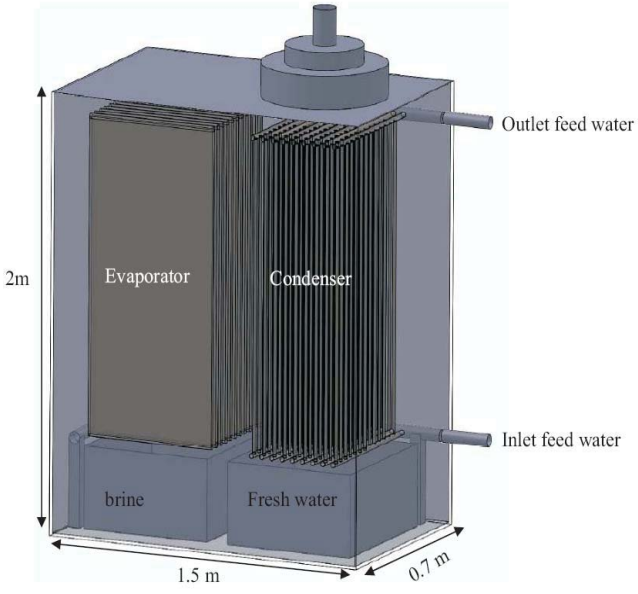

Fig. 2. Schematic diagram of the distillation module designed with Solidworks software.

Table 1
Properties of the distillation module components used in simulation

Components	Description	Value/Type
Evaporation chamber	Size	0.5 × 0.5 × 1.5 m³
	Packing	Textile
	Exchange surface	49 m²
	Mass transfer coefficient	$K_m = \frac{\left(2.09 m_{l,\mathrm{ev}}^{0.45}\ m_{g,\mathrm{ev}}^{0.11515}\right)}{a_{\mathrm{ev}}}$
	Heat transfer coefficient	$h_L = \frac{\left(5{,}900 m_{l,\mathrm{ev}}^{0.169}\ m_{g,\mathrm{ev}}^{0.5894}\right)}{a_{\mathrm{ev}}}$
	Air-film heat transfer coefficient	$h_g = C_{g,\mathrm{ev}} K_m$
	Heat transfer coefficient	$h_L = \frac{\left(5{,}900 m_{l,\mathrm{ev}}^{0.169}\ m_{g,\mathrm{ev}}^{0.5894}\right)}{a_{\mathrm{ev}}}$
Condensation chamber	Size	0.5 × 0.5 × 1.5 m³
	Tubes type	Copper
	Inner diameter, d_i	0.014 m
	Outer diameter, d_e	0.012 m
	Tube length, L	1.5 m
	Transverse pitch, P_t	0.050 m
	Longitudinal pitch, P_1	0.050 m

3. Theoretical analysis

3.1. Mathematical model development

The first stage of all survey of a thermal process requires its representation by a mathematical model. This model must characterize the real behavior of the studied system. The distillation module may be modeled as shown in Fig. 3. Air flow rate enters the bottom of the evaporation chamber at a temperature $T_{g1,\mathrm{ev}}(t)$ and a humidity $W_{g1,\mathrm{ev}}(t)$. The mass velocity of air is $m_{\mathrm{g,ev}}(t)$. The air flow rate exits at the top of the evaporation tower at a temperature $T_{g2,\mathrm{ev}}(t)$ and a humidity $W_{g2,\mathrm{ev}}(t)$. Hot water coming from solar water collector is pulverized at the top of the tower with a temperature $T_{l2,\mathrm{ev}}(t)$ and no evaporated water is in the bottom of the tower with a temperature $T_{l1,\mathrm{ev}}(t)$. The mass velocity of water is $m_{l,\mathrm{ev}}(t)$. The humid air, in provenance from the evaporator, enters

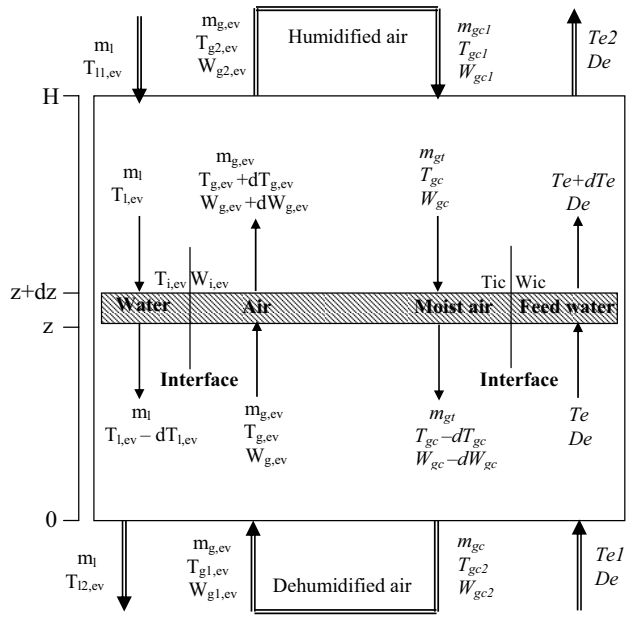

Fig. 3. An element of volume of the distillation module.

the condenser by the top at temperature $T_{gc2}(t)$, humidity $W_{gc2}(t)$ and mass flow rate $m_{gt}(t)$. The cooling water is introduced at the bottom of the condenser at temperature $T_{e1}(t)$ and a mass flow rate $D_e(t)$.

The method of setting up the heat and mass balances will be undertaken with the following simplifying assumptions:

- The process is adiabatic.
- The air and water flows are in countercurrent and one dimensional.
- The specific heat of water is constant during its passage by the distillation module.
- The humid air is considered as a perfect gas.
- Water phase at the evaporation chamber:

$$\frac{\partial T_{l,\mathrm{ev}}}{\partial t}=\frac{m_l}{M_{l,\mathrm{ev}}}\times\frac{\partial T_{l,\mathrm{ev}}}{\partial z}-\frac{h_l a_{\mathrm{ev}}}{M_{l,\mathrm{ev}}C_l}\left(T_{l,\mathrm{ev}}-T_{l,\mathrm{ev}}\right) \tag{1}$$

- Air phase at the evaporation chamber:

$$\frac{\partial T_{g,\mathrm{ev}}}{\partial t}=\frac{m_{g,\mathrm{ev}}}{M_{g,\mathrm{ev}}}\times\frac{\partial T_{g,\mathrm{ev}}}{\partial z}-\frac{h_g a_{\mathrm{ev}}}{M_{g,\mathrm{ev}}C_{g,\mathrm{ev}}}\left(T_{g,\mathrm{ev}}-T_{l,\mathrm{ev}}\right) \tag{2}$$

- The air–water interface at the evaporation chamber:

The following equation gives the balance of mass at the level of interfacing air water:

$$\frac{\partial W_{g,\mathrm{ev}}}{\partial t}=-\frac{m_{g,\mathrm{ev}}}{M_{g,\mathrm{ev}}}\times\frac{\partial W_{g,\mathrm{ev}}}{\partial z}+\frac{K_m a_{\mathrm{ev}}}{M_{g,\mathrm{ev}}}\left(W_{l,\mathrm{ev}}-W_{g,\mathrm{ev}}\right) \tag{3}$$

The balance of heat at the level interfacing air–water is given by the following equation:

$$h_l a_{\mathrm{ev}}\left(T_{l,\mathrm{ev}}-T_{l,\mathrm{ev}}\right)=h_g a_{\mathrm{ev}}\left(T_{l,\mathrm{ev}}-T_{g,\mathrm{ev}}\right)+\lambda_o K_m a_{\mathrm{ev}}\left(W_{l,\mathrm{ev}}-W_{g,\mathrm{ev}}\right) \tag{4}$$

- Water phase at the condensation chamber:

$$\frac{\partial T_e}{\partial t}=-\frac{m_e}{M_e}\times\frac{\partial T_e}{\partial z}+\frac{UA_c}{M_e C_e}\times\left(T_{\mathrm{Ic}}-T_e\right) \tag{5}$$

- Air phase at the condensation chamber:

$$\frac{\partial T_{\mathrm{gc}}}{\partial t}=\frac{m_{\mathrm{gt}}}{M_{\mathrm{gc}}}\times\frac{\partial T_{\mathrm{gc}}}{\partial z}-\frac{h_{\mathrm{gc}}A_c}{M_{\mathrm{gc}}C_{\mathrm{gc}}}\left(T_{\mathrm{gc}}-T_{\mathrm{Ic}}\right)-\frac{\lambda_o K_{\mathrm{mc}}A_c}{M_{\mathrm{gc}}C_{\mathrm{gc}}}\left(W_{\mathrm{gc}}-W_{\mathrm{Ic}}\right) \tag{6}$$

- Air–condensate interface

The following equation gives the heat balance at the air–condensate interface:

$$h_{\mathrm{gc}}A_c\left(T_{\mathrm{gc}}-T_{\mathrm{ic}}\right)+UA_c\left(T_{\mathrm{ic}}-T_e\right)=\lambda_o K_{\mathrm{mc}}A_c\left(W_{\mathrm{gc}}-W_{\mathrm{ic}}\right) \tag{7}$$

The mass balance at air–condensate interface is given by the following equation:

$$\frac{\partial W_{\mathrm{gc}}}{\partial t}=\frac{m_{\mathrm{gt}}}{M_{\mathrm{gc}}}\times\frac{\partial W_{\mathrm{gc}}}{\partial z}+\frac{K_{\mathrm{mc}}A_c}{M_{\mathrm{gc}}}\left(W_{\mathrm{gc}}-W_{\mathrm{Ic}}\right) \tag{8}$$

The water condensation rate is determined by using an algebraic equation that relates the variation of the water content with the height of the tower:

$$dm_c=K_{\mathrm{mc}}A_c\left(W_{\mathrm{Ic}}-W_{\mathrm{gc}}\right)dz \tag{9}$$

3.2. Mathematical model approximation

The analytical solution of Eqs. (1)–(9) is impossible and they must be discretized to obtain approximate, but still accurate, solutions. The orthogonal collocations method (OCM) approximates the solution by a polynomial trial function, and the resulting set of the ordinary differential equations (ODE) is often considerably smaller [15,16]. The set of partial differential equations is transformed to the following set of ODE using the OCM with the boundary conditions: $0 \le z \le H$.

$$T_{l,\mathrm{ev}}\left(H,t\right)=T_{l1,\mathrm{ev}}\left(t\right),\ T_e\left(0,t\right)=T_{e1}\left(t\right)$$

$$T_{g,\mathrm{ev}}\left(0,t\right)=T_{g1,\mathrm{ev}}\left(t\right),\ T_{\mathrm{gc}}\left(H,t\right)=T_{\mathrm{gc1}}\left(t\right)$$

$$W_{g,\mathrm{ev}}\left(0,t\right)=W_{g1,\mathrm{ev}}\left(t\right),\ W_{\mathrm{gc}}\left(H,t\right)=W_{\mathrm{gc1}}\left(t\right)$$

The expression of the distillation module-reduced dynamic model is given by the following equations:

$$\frac{dT_{l,\mathrm{evi}}}{dt}=\frac{m_l}{M_{l,\mathrm{ev}}}\left[\sum_{j=0}^{N}l_{\mathrm{ij}}T_{l,\mathrm{evj}}+l_{iN+1}T_{l,\mathrm{ev2}}\right]-\frac{h_l a_{\mathrm{ev}}}{M_{l,\mathrm{ev}}C_l}\left(T_{l,\mathrm{ev}}-T_{l,\mathrm{evi}}\right) \tag{10}$$

$$\frac{dT_{g,\mathrm{evi}}}{dt}=-\frac{m_{g,\mathrm{ev}}}{M_{g,\mathrm{ev}}}\left[\sum_{j=1}^{N+1}l_{\mathrm{ij}}T_{g,\mathrm{evj}}+l_{i0}T_{g,\mathrm{ev0}}\right]-\frac{h_g a_{\mathrm{ev}}}{M_{g,\mathrm{ev}}C_{g,\mathrm{ev}}}\left(T_{g,\mathrm{evi}}-T_{l,\mathrm{ev}}\right) \tag{11}$$

$$\frac{dW_{g,\mathrm{evi}}}{dt} = -\frac{m_{g,\mathrm{ev}}}{M_{g,\mathrm{ev}}}\left[\sum_{j=1}^{N+1} l_{\mathrm{ij}} W_{g,\mathrm{evj}} + l_{i0} W_{g,\mathrm{ev0}}\right] + \frac{K_m a_{\mathrm{ev}}}{M_{g,\mathrm{ev}}}\left(W_{I,\mathrm{ev}} - W_{g,\mathrm{evi}}\right) \quad (12)$$

$$h_l a_{\mathrm{ev}}\left(T_{l,\mathrm{ev}} - T_{l,\mathrm{evi}}\right) = h_g a_{\mathrm{ev}}\left(T_{I,\mathrm{ev}} - T_{g,\mathrm{evi}}\right) + \lambda_o K_m a_{\mathrm{ev}}\left(W_{I,\mathrm{ev}} - W_{g,\mathrm{evi}}\right) \quad (13)$$

$$\frac{dT_{\mathrm{ei}}}{dt} = -\frac{D_e}{M_e}\left[\sum_{j=1}^{N+1} l_{\mathrm{ij}} T_{\mathrm{ei}} + l_{i0} T_{e1}\right] + \frac{UA_c}{M_e C_e}\left(T_{\mathrm{Ic}} - T_{\mathrm{ei}}\right) \quad (14)$$

$$\frac{dT_{\mathrm{gci}}}{dt} = \frac{m_{\mathrm{gt}}}{M_{\mathrm{gc}}}\left[\sum_{j=0}^{N} l_{\mathrm{ij}} T_{\mathrm{gci}} + l_{iN+1} T_{\mathrm{gc2}}\right] - \frac{h_{\mathrm{gc}} A_c}{M_{\mathrm{gc}} C_{\mathrm{gc}}}\left(T_{\mathrm{gci}} - T_{\mathrm{Ic}}\right) - \frac{\lambda_o K_{\mathrm{mc}} A_c}{M_{\mathrm{gc}} C_{\mathrm{gc}}}\left(W_{\mathrm{gci}} - W_{\mathrm{Ic}}\right) \quad (15)$$

$$\frac{dW_{\mathrm{gci}}}{dt} = \frac{m_{\mathrm{gt}}}{M_{\mathrm{gc}}}\left[\sum_{j=0}^{N} l_{\mathrm{ij}} W_{\mathrm{gci}} + l_{iN+1} W_{\mathrm{gc2}}\right] + \frac{K_{\mathrm{mc}} A_c}{M_{\mathrm{gc}}}\left(W_{\mathrm{gci}} - W_{\mathrm{Ic}}\right) \quad (16)$$

$$h_{\mathrm{gc}} A_c\left(T_{\mathrm{gci}} - T_{\mathrm{Ic}}\right) + UA_c\left(T_{\mathrm{Ic}} - T_{\mathrm{ei}}\right) = \lambda_o K_{\mathrm{mc}} A_c\left(W_{\mathrm{gci}} - W_{\mathrm{Ic}}\right) \quad (17)$$

$$\frac{dm_c}{dz} = K_{\mathrm{mc}} A_c\left(W_{\mathrm{Ic}} - W_{\mathrm{gci}}\right) \quad (18)$$

where $i = 1, 2, 3, \ldots, N + 1$.

3.3. Algorithm of the model solution

A computer simulation program was compiled in terms of the distillation module model to determine the air and water temperatures, the amount of water in the air at the outlet of the distillation module as a function of water and air temperatures, air mass flow rate, water mass flow rate and absolute humidity at the inlet of the distillation module. Eqs. (10)–(18) were solved using the fourth-order Runge–Kutta method. In the computer program, water and air flow rates and an initial guess of all the temperatures were introduced as an input to the computer simulation program. The accuracy criterion (taken equal to 0.00001) and the distillation module height was divided into $n = 6$ collocation points. Hence, the number of equations to be solved was also introduced to the simulation program. The operating variables are air and water temperatures, absolute and humidity, heat and mass transfer coefficients and evaporation chamber efficiency. They were calculated at each collocation point until a specified accuracy was achieved.

4. Simulation results

Figs. 4 and 5 show the effect of air and water inlet temperatures and the height of the packed bed, respectively, on the outlet absolute humidity of the air stream inside the distillation module. The simulation results depicted in Fig. 4 were obtained by fixing the inlet air temperature while different values for inlet water temperature values were introduced to the simulation program and vice versa. The obtained results illustrate that the absolute outlet humidity of the air stream increases with increasing air and water inlet temperatures. This is because increases in water or air inlet temperature rises the gradient temperature between air and water inside the humidifier which in its turn leads to increasing the mass and heat transfer coefficients and then its outlet parameters. It is also noticeable from these simulation results that the absolute outlet humidity is more affected by the inlet water temperature than the inlet air one. Therefore, according to these results, one can infer the interest of working with high values of inlet water temperature at the inlet of the evaporation tower instead of high values of inlet air temperature to allow the latter to provide high values of absolute air humidity. Fig. 5 presents the effect of the height of the packed bed used in the evaporation tower (textile of viscose) on the outlet absolute humidity of the air stream. In this study, all the parameters were fixed while different values for the height of the packed bed were introduced to the simulation program. It is clear from the figure that the outlet humidity absolute could be increased significantly if the packed bed surface area is increased. The same trend was found by Ben Amara [17].

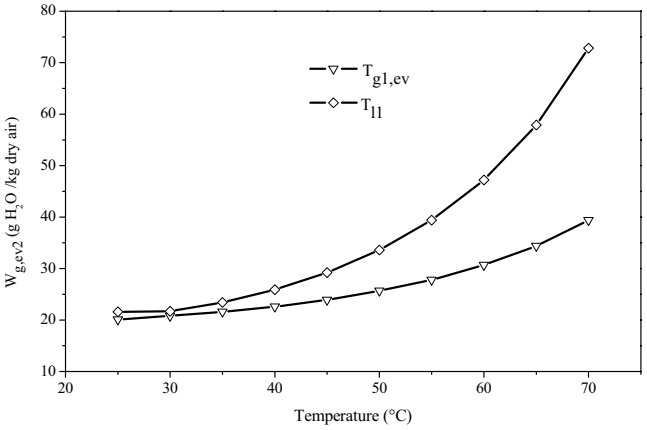

Fig. 4. Variation outlet absolute humidity of the air stream versus air and water inlet temperatures.

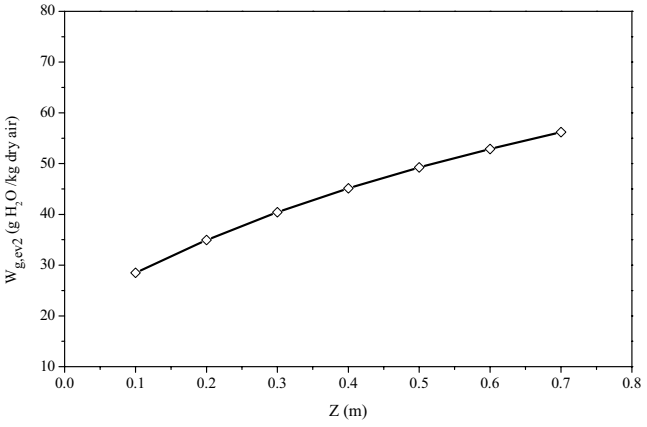

Fig. 5. Variation of outlet absolute humidity of the air stream versus the height of the the packed bed.

Figs. 6–8 show the variation of the amount of evaporated water, m_{ev}, inside the distillation module as a function,

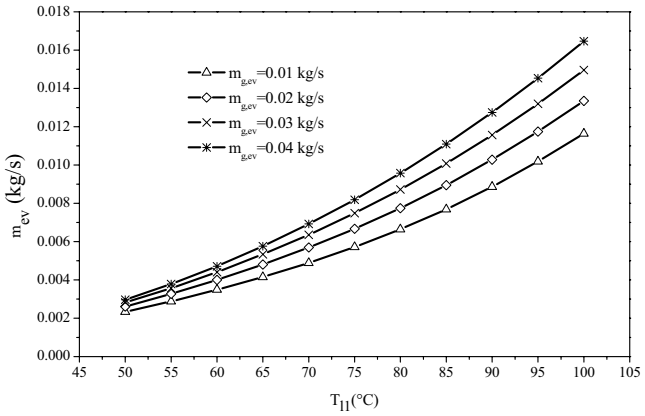

Fig. 6. Variation of evaporated amount water versus inlet water temperature and air flow rate.

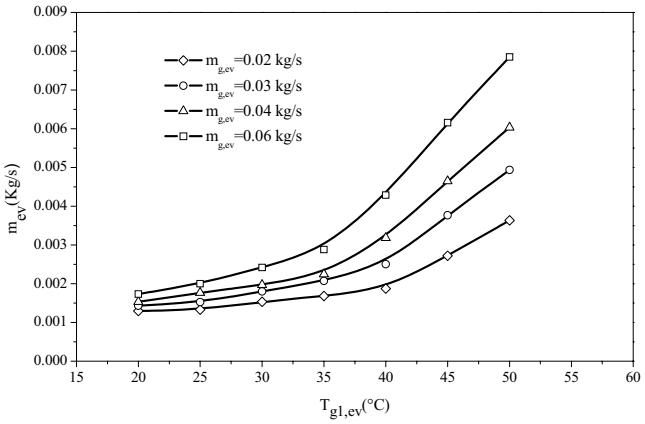

Fig. 7. Variation of evaporated amount water versus inlet air temperature and air flow rate.

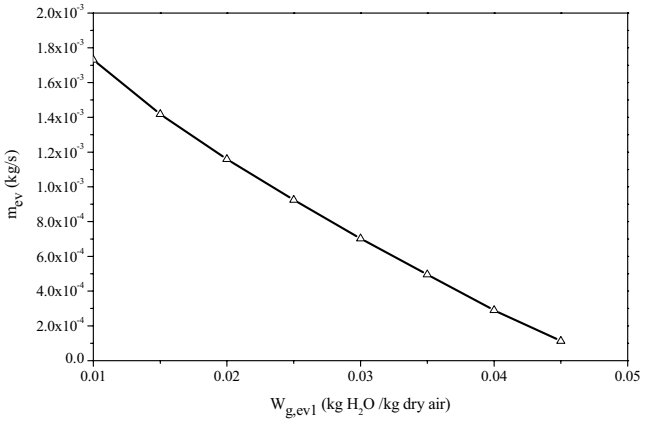

Fig. 8. Variations of evaporated amount water versus inlet absolute air humidity.

respectively, of water and air inlet temperatures for different values of air flow rates and inlet absolute humidity. Results depicted in Fig. 6 show that the amount of evaporated water increases with increasing inlet water temperature and air flow rate. This can be explained by the fact that increases inlet water temperature increases the gradient temperature between air and water inside the distillation module which in its turn leads to increasing the mass and heat transfer coefficients and then the amount of evaporated water. Fig. 7 reveals that the amount of evaporated water increases with the inlet air temperature. The heating air inside the evaporation chamber increases its capacity to load water vapor thus resulting in the high amount of evaporated water. According to the Fig. 8, it was found that the amount of evaporated water decreases as the inlet absolute air humidity increases, apparently due to the low capacity of the air stream to load water vapor.

Figs. 9 and 10 present the variation of the humidification efficiency, ε, and the amount of evaporated water, m_{ev}, as a function of operating parameters. The humidification efficiency is defined as [18–20]:

$$\varepsilon = \frac{W_{g1,ev} - W_{g2,ev}}{W_{g1,ev} - W_{I,ev}} \tag{19}$$

where $W_{g1,ev}$, and $W_{g2,ev}$ are, respectively, the absolute humidity of air at the inlet and the outlet of the evaporator. $W_{I,ev}$ represents the absolute humidity at saturation state calculated by using the following empirical correlation [21].

$$W_{I,ev} = \frac{0.622}{\frac{P_{amb}}{910^{-6}T_{g,ev}^4 - 0.0003T_{g,ev}^3 + 0.0406T_{g,ev}^2 - 0.1179T_{g,ev} + 10.738} - 1} \tag{20}$$

where P_{amb} shows the ambient air pressure.

Fig. 9 shows the variation of distillation module humidification efficiency versus inlet water temperature at the evaporation tower for different values of water flow rates. It is clear from the obtained curves that increasing the evaporator inlet water temperature decreased the values of humidification efficiency. However, increasing water flow rates increased the humidification efficiency. This result is due to the fact that higher water flow rate will improve both the mass transfer rate and the degree of wetting of

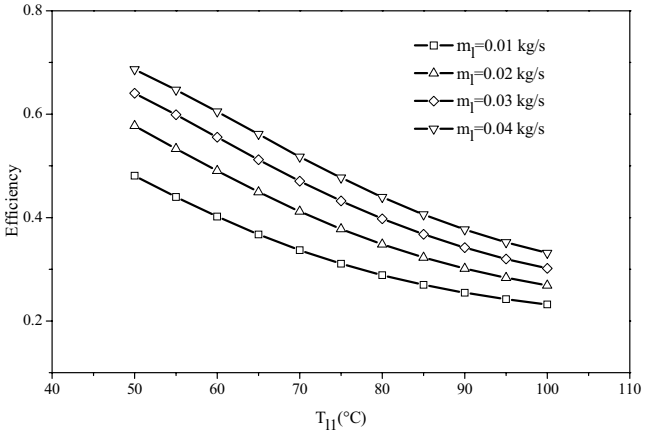

Fig. 9. Variation of distillation module efficiency versus inlet water temperature and water flow rate.

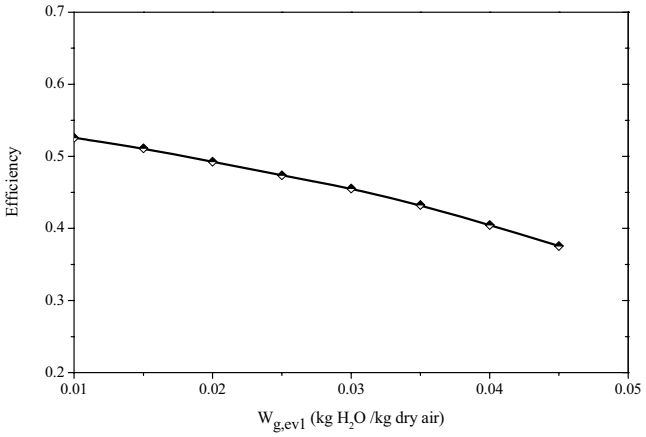

Fig. 10. Variations of humidification efficiency versus inlet absolute air humidity.

Fig. 11. A photo of the solar desalination unit experimental setup.

packing [22]. Variation of humidification efficiency versus inlet absolute air humidity is depicted in Fig. 10. The result shows that increasing inlet absolute air humidity decreases the humidification efficiency.

5. Experimental validation of the distillation module

The experimental validation of the mathematical model developed for the distillation module is a very important consideration because it determines whether the mathematical model is a faithful representation of the actual physical system and indicates the level of accuracy that may be expected in the predictions obtained from the model. In order to validate the developed model of the distillation module, a series of experiments was conducted using the pilot desalination unit, as shown in Fig. 11, located at the National Engineering School of Sfax (ENIS)—Sfax University, Tunisia. Experimental measurements were taken on the distillation module (evaporation and condensation chambers) shown in Fig. 12. Table 2 presents some experimental measurement of average values of the main parameters in the distillation module.

The distillation module was equipped with Pt 100 thermistors with a sensibility of 0.3799X/°C for measuring the outlet and the inlet water and air temperatures. All the sensors, which were calibrated before using to determine the probes sensibility, were connected to a data acquisition system (type Agilent 34970A). During experimentation, all the parameters were measured and recorded every 1 min for up to 420 min. All the measurements started at 10:30 a.m.

Table 2
Experimental average values of the main parameters in the distillation module

I (W/m^2)	T_{amb} (°C)	$\dot{m}_{g,ev}$(kg/s)	$\dot{m}_l$ (kg/s)	$f_{1,ev}$ (%)	$f_{2,ev}$ (%)	$T_{g1,ev}$ (°C)	$T_{l2,ev}$ (°C)	$\dot{m}_c$ (kg/day)
536	32	0.01	0.04	7,541	49,339	54.6	45.55	16
602	31.89	0.0103	0.03	12,487	51,070	55.9	69.57	18.5
576	30.75	0.01	0.045	8,805	49,817	54.67	59.70	17.12
693	32.75	0.01	0.04	11,480	50,126	53.60	44.69	21.75
574	32.69	0.0074	0.07	18,547	56,936	52.86	39.17	17
569	35.05	0.0092	0.07	18,718	57,195	57.14	39.07	16.75
621	34.89	0.0092	0.07	20,210	57,340	56.65	41.65	18.85
653	36	0.0103	0.07	21,755	57,669	60.77	45	20.25
635	37.30	0.0103	0.02	20,940	57,584	60.85	48.95	19.25
584	37.48	0.0088	0.02	20,835	57,472	57.78	60.64	17.25
635	33.502	0.0103	0.03	22,403	58,221	52.20	71.70	19.75
656	35.16	0.0103	0.03	26,114	58,840	60.81	54.12	20.5
588	41.95	0.0103	0.03	24,231	58,389	56.90	62.97	17.5
671	37.02	0.0074	0.03	28,322	59,230	58.58	64.10	21
689	36.59	0.0103	0.03	29,951	59,255	62.48	63.10	21.25
624	39.29	0.0166	0.036	29,018	59,187	59.52	51.77	19
572	35.32	0.0166	0.03	26,931	59,151	55.20	66.53	17

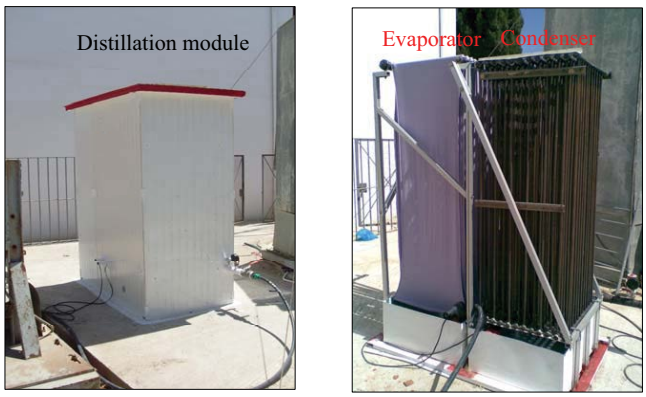

Fig. 12. Outside and inside photos of the realized distillation module.

Figs. 13 and 14 present a comparison between predicted and measured values, respectively, of air and water outlet temperatures and the absolute humidity at the level of the humidifier. According to these figures, the experimental and simulation variations are identical for almost the entire period. In addition, water and air outlet temperatures of the distillation module present only a small change during the variation of the solar radiation for both experimental and numerical tests. The accuracy of the experimental results may be calculated using the following definition:

$$\varepsilon_{ar}(\%) = \frac{100}{k} \times \sum_{i=1}^{k} \frac{\left|T_{exp}(i) - T_{sim}(i)\right|}{T_{exp}(i)} \quad (21)$$

The error analysis of the studied parameters is presented in Table 3. It is seen in this table that the agreement between experiment data and the results calculated from the theoretical prediction of the present device is fairly good. The uncertainty in the experimental results presented in this work is estimated using the approach described by Barford [23] and Moffat [24]. The uncertainty in the measurements is defined as the root sum square of the fixed error of the instrumentation and the random error observed during different measurements. The systematic experimental error for temperature is ±0.5°C.

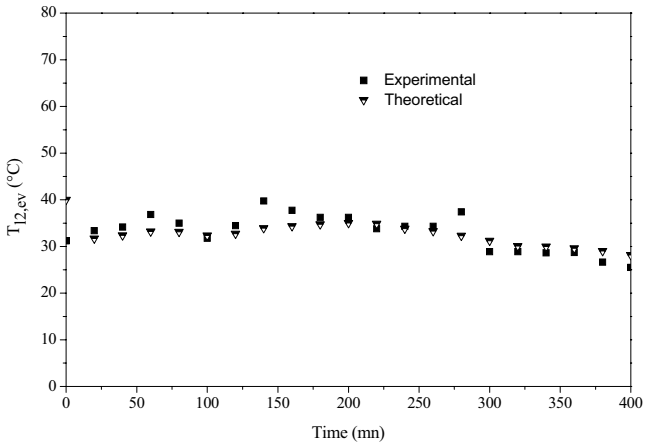

Fig. 13. Comparisons between numerical and experimental values of water temperature at the evaporation chamber exit.

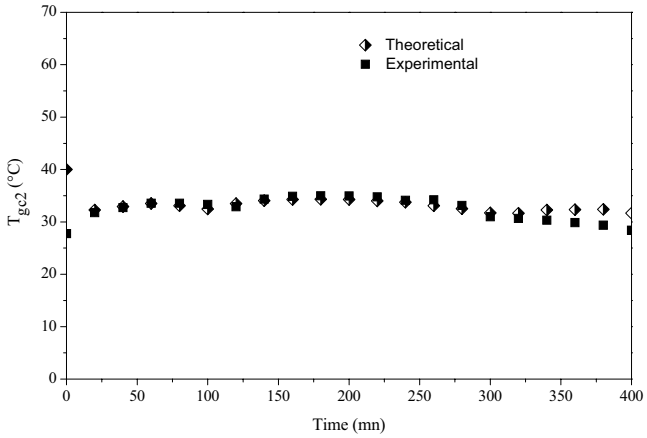

Fig. 14. Comparisons between numerical and experimental values of air temperature at the condensation chamber exit.

Table 3
The accuracy of the experimental results

Parameter	Average relative error ε_{ar} (%)	Maximum absolute error ε_{max} (°C)	Minimum absolute error ε_{min} (°C)
$T_{l2,ev}$	5.382	9.995	3.91×10^{-2}
T_{gc2}	2.101	3.317	3.29×10^{-3}

Note: $\varepsilon_{max} = \max\left|T_{exp}(i) - T_{sim}(i)\right|$, $\varepsilon_{min} = \min\left|T_{exp}(i) - T_{sim}(i)\right|$, $i = 1, 2, \ldots k$

The good agreement between experimental and simulation results demonstrate the validity of the mathematical model established for the distillation module and the effectiveness of the orthogonal collocation method used to solve them. In addition, the validated mathematical model would help in the development of computer-based design and simulation software for such type of distillation module.

6. Conclusion

This paper focuses on the theoretical and experimental studies of a distillation module used in a solar desalination unit utilizing the humidification and dehumidification principle. The first part of the study deals with the presentation of the designed and constructed distillation module. In the second part, a mathematical model based on heat and mass balances for air and water inside the distillation module is presented. The developed model is simulated using the Borland C++ software to study the influence of operating parameters on both the humidification efficiency of the distillation module and the amount of evaporated water. The predicted and the measured parameters are in good agreement. From the results and discussions, the following conclusions can be drawn:

- The absolute outlet humidity of the air stream increases with increasing air and water inlet temperatures.
- The absolute outlet humidity is more affected by the inlet water temperature than the inlet air one.

- Increasing the inlet water and air temperatures to the evaporation chamber increases the amount of evaporated water.
- Increasing the evaporator inlet water temperature decreases the humidification efficiency.
- Increasing the inlet absolute air humidity decreases the amount of evaporated water and the humidification efficiency.
- Increasing water flow rate increases the humidification efficiency.

The above findings from the experimental and theoretical studies of the distillation module can serve as a blueprint for future attempts to optimize and improve the design parameters influencing the performance of the distillation module. In addition, the validated mathematical models would help in the development of a computer-based design and simulation software for such type of distillation module.

Acknowledgments

The authors would like to thank the Ministry of Higher Education, Scientific Research and Information and Communication Technologies MESRS-TIC for its financial support to the R&D project entitled "Solar Driven Membrane Distillation for Resource Efficient Desalination in Remote Areas" and the Fraunhofer Institute for Solar Energy Systems ISE for its collaboration.

Symbols

A — Air–water exchanger area in the condensation tower, m^2
a — Air–water exchanger area, m^2
C_e — Water-specific heat, J/(kg K)
C_f — Fluid specific heat, J/(kg K)
C_g — Moist air specific heat in the humidifier, J/(kg K)
C_{gc} — Moist air specific heat in the condensation tower, J/(kg K)
$C_{g,ev}$ — Moist air specific heat in the evaporation tower, J/(kg K)
D_e — Water mass velocity in the condensation tower, kg/(m^2 s)
h — Heat transfer coefficient, J/(kg K)
h_g — Air heat transfer coefficient at the air–water interface, W/(m^2 K)
h_e — Water heat transfer coefficient at the air–water interface, W/(m^2 K)
k — Number of experimental measurements
K — Thermal conductivity, W/(m K)
K_m — Water vapor mass transfer coefficient at the air–water interface, kg/(m^2 s)
m — Mass flow rate, kg/s
m_c — Fresh water production, kg/s
m_{gt} — Total mass velocity of moist air in the condenser, kg/(m^2 s)
f — Relative humidity (%)
P_i — Saturation pressure, Pa
T — Temperature, K
T_{exp} — Experimental value of temperature, °C
T_i — Temperature at the air–water interface, K
T_{sim} — Theoretical prediction of temperature, °C
U — Overall heat transfer coefficient in the condensation tower, W/(m^2 K)
W — Air humidity, kg water/kg dry air
W_i — Saturation humidity, kg water/kg dry air
z — Coordinate in the flow direction, m
λ_o — Latent heat of water evaporation, J/kg
e — Error

Subscripts

1 — Tower bottom
2 — Tower top
a — Air
c — Condensation tower
e — Cooling water
ev — Evaporation tower
g — Moist air
w — Water

References

[1] H.P. Garg, H.S. Mann, Effect of climatic, operational and design parameters on the year round performance of single-sloped and double-sloped solar still under Indian arid zone conditions, Solar Energy, 18 (1976) 159–163.
[2] A.K. Rajvanshi, Effect of various dyes on solar distillation, Solar Energy, 27 (1981) 51–65.
[3] G.M. Zaki, A.M. Radhwan, A.O. Balbeid, Analysis of assisted coupled solar still, Solar Energy, 27 (1981) 51–65.
[4] A. Delyannis, The Patmos solar distillation plant, Solar Energy, 11 (1968) 113–115.
[5] V.A. Baum, R. Bairamov, Prospects of solar stills in Turkmenia, Solar Energy, 10 (1966) 38–40.
[6] K. Srithar, T. Rajaseenivasan, Recent fresh water augmentation techniques in solar still and HDH desalination – a review, Renew. Sustain. Energy Rev., 82 (2018) 629–644.
[7] M. Chandrashekara, A. Yadav, Water desalination system using solar heat: a review, Renew. Sustain. Energy Rev., 67 (2017) 1308–1330.
[8] P. Behnam, M.B. Shafii, Examination of a solar desalination system equipped with an air bubble column humidifier, evacuated tube collectors and thermosyphon heat pipes, Desalination, 397 (2016) 30–37.
[9] C. Muthusamy, K. Srithar, Energy and exergy analysis for a humidification–dehumidification desalination system integrated with multiple inserts, Desalination, 367 (2015) 49–59.
[10] S. Malek, Experimental analysis of solar still with external condenser, Int. J. Recent Innov. Trends Comput. Commun. (IJRITCC), 2 (2014) 983–986.
[11] E.W. Tow, J.H. Lienhard V, Experiments and modeling of bubble column dehumidifier performance, Int. J. Therm. Sci., 80 (2014) 65–75.
[12] A.M. Shawesh, A Study of Heat and Mass Transfer in Dual Water Heater, Thesis, http://digitool.Library.McGill.CA:80/R/-?func=dbin-jump-full&object_id=20519&silo_library=GEN01.
[13] K. Zhani, H. Ben Bacha, T. Damak, Modeling and experimental validation of a humidification and dehumidification desalination unit solar part, Desal. Water Treat., 5 (2011) 3159–3169.
[14] K. Zhani, H. Ben Bacha, Modeling, simulation and experimental validation of a pad humidifier used in solar desalination process, Desal. Water Treat., 7–9 (2013) 1477–1486.
[15] T. Damak, Modeling, Estimation and Control of Biotechnological Processes of Hyperbolic Type, PhD Thesis, Paul Sabatier University, Toulouse, France, 1994.
[16] R.K. Srivastava, B. Joseph, Reduced-order model for separation columns. V. Selection of collocation points, Comput. Chem. Eng., 9 (1985) 601–613.

[17] M. Ben Amara, Study of Water Desalination by Multi-stage Humidification-Dehumidification, PhD Thesis, Faculty of Sciences of Tunis, University of Tunis El-manar, Tunis, 2005.
[18] E. Chafik, A new seawater desalination process using solar energy, Desalination, 153 (2002) 25–37.
[19] J. Orfi, M. Laplante, H. Marmouch, N. Galanis, B. Benhamou, S. Ben Nasrallah, C.T. Nguyen, Experimental and theoretical study of a humidification–dehumidification water desalination system using solar energy, Desalination, 168 (2004) 151–159.
[20] Agricultural University of Athens, 10th Deliverable: Experimental optimization of humidifiers design of an optimized humidifier prototype, EU Contract No. IC18-CT98-0265, January 2001.
[21] M. Ben Amara, A. Ben Ezzine, I. Houcine, A.A. Guizani, M. Maalej, Development and Characterization of Flat Air Solar Collectors Used in a Process of Desalination by Humidification–Dehumidification of Air, Proc. 4th Tunisian Days on Flows and Transfers JTET 2002, Hammamet, 2 December, 2002, pp. III.21–III.28.
[22] S. Yanniotis, K. Xerodemas, Air humidification for seawater desalination, Desalination, 158 (2003) 313–319.
[23] N.C. Barford, Experimental measurements: precision, error and truth, 2nd ed., John Wiley & Sons, New York, 1990.
[24] R.J. Moffat, Describing the uncertainties in experimental results, Exp. Therm. Fluid Sci., 1 (1988) 3–17.